# Magnetostriction of PdFe alloys

J. E. Schmidt and L. Berger

Citation: Journal of Applied Physics **55**, 1073 (1984); doi: 10.1063/1.333190
View online: http://dx.doi.org/10.1063/1.333190
View Table of Contents: http://scitation.aip.org/content/aip/journal/jap/55/4?ver=pdfcov
Published by the AIP Publishing

# Magnetostriction of Pd-Fe alloys

J. E. Schmidt[a] and L. Berger
*Physics Department, Carnegie-Mellon University, Pittsburgh, Pennsylvania 15213*

(Received 22 August 1983; accepted for publication 29 September 1983)

The linear magnetostriction $\lambda_s$ of polycrystalline $Pd_{1-x}Fe_x$ alloys has been measured as a function of alloy composition, at temperatures of 300, 77, and 4.2 K. The effect on $\lambda_s$ of atomic ordering of $Pd_3Fe$ and PdFe type has been investigated. The value of $\lambda_s$ is positive for $x > 0.21$, but changes sign three times in the composition range $x < 0.21$. This composition dependence can be understood semiquantitatively in terms of the simple split-band model, where iron and palladium each have their own $d$ band, distinct on the energy scale. Contributions to $\lambda_s$ from electrons of both spin directions have been included. Best fit between theory and data is obtained for a value of the deformation potential of $d$ electrons equal to $-0.6$ eV. The anomalous Hall effect and the $g$ factor of Pd-Fe are also discussed in the light of the split-band model.

PACS numbers: 75.80. + q, 75.50.Bb

## I. INTRODUCTION

At the start of this research, only a few data points[1,2] for the magnetostriction of $Pd_{1-x}Fe_x$ alloys existed. Since then, the work of Fukamichi and collaborators on bulk alloys at 300 K has appeared,[3,4] as well as the work of Lee and collaborators[5] on thin films at 300 K.

We have measured the linear magnetostriction $\lambda_s$ at 300, 77, and 4.2 K, over the whole binary alloy series. We have investigated the effect of atomic ordering on $\lambda_s$, through water-quenching treatments and long anneals. Also, we have considered with special care the range of iron atomic fraction between $x = 0$ and $x = 0.21$, where we have discovered that several changes of sign of $\lambda_s$ take place.

The physical properties of Pd-Fe alloys are similar[6] to those of Ni-Fe. However, the saturation magnetization of Pd-Fe falls below the well-known Slater–Pauling curve at iron atomic fractions smaller than $x \cong 0.20$, indicating that the spin-up $d$ band is not full anymore. The rapid motion of the Fermi level through the spin-up $d$ band explains the multiplicity of the sign changes of $\lambda_s$ in that composition range.

## II. DESCRIPTION OF SAMPLES AND EXPERIMENTAL APPARATUS

Our samples were made from Johnson–Matthey iron rods, "Specpure" grade, and from Materials Research Corporation palladium slugs, "Marz" grade. These materials were rolled into thin strips in a small rolling mill. The iron and palladium strips were wrapped around each other to ensure good physical contact, thus lowering the effective melting temperatue below that of the pure elements. Melting was done in a small molybdenum resistance furnace in a vacuum of $10^{-5}$ Torr, using recrystallized $Al_2O_3$ crucibles. Weight loss by evaporation or splashing varied between 0.4% and 4%. The ingots were cold-rolled into strips of thickness between 0.4 and 1.2 mm, which were cut into rectangles of length 34 mm and width 5–10 mm. These samples were homogenized at 1100 °C in a vacuum of $10^{-6}$ Torr for 20 h.

Two different kinds of atomic ordering can occur in the $Pd_{1-x}Fe_x$ system. The $Pd_3Fe$ type of ordering, similar to $Cu_3Au$, is observed[7] in fcc alloys for $x$ between $\cong 0.20$ and 0.37. In fcc alloys at $x$ between $\cong 0.37$ and 0.55, the PdFe type of ordering, similar to CuAu, takes place.[7] This ordered phase is tetragonally distorted. Between $x \cong 0.55$ and $x \cong 0.98$, a bcc phase coexists with the face-centered phase. Above $x \cong 0.98$, the bcc phase exists alone.

The final thermal treatment given to the samples after homogenization is either treatment (a) or treatment (d). Treatment (a) consists of an anneal for 2 h in a $10^{-5}$ Torr vacuum at 1100 °C in a quartz tube, followed by quenching in water under atmospheric pressure. Treatment (d) is an anneal for 20 h in a $10^{-5}$ Torr vacuum at 550 °C, followed by rather slow furnace cooling; however, the samples with $x = 0.03$–$0.18$ were annealed at temperatures falling in stages from $\cong 450$ °C to $\cong 300$ °C, because of their lower ordering temperature. Quench (a) is designed to minimize the degree of atomic ordering, and anneal (d) to maximize it. Changes in the degree of order were monitored by measuring the electrical resistivity of some samples.[6]

In addition, quench (a) tends to retain the fcc phase in the normally two-phase $0.55 < x < 0.70$ range.

Atomic absorption spectroscopy is used to check the iron concentration of all samples. The measured concentration agrees with the nominal concentration within the random dispersion of the measurements. From now on, we quote the nominal values.

Electron microprobe analysis was performed on some samples, with an electron beam 1 $\mu$m in diameter. It shows that the iron concentration varies along the length of the sample by no more than $\pm$ 1% of its average value.

The magnetostriction is measured[8] with Pt-W strain gages manufactured by Dentronics, Inc. (Model AP 1832 NE). These have the advantage of remaining nonmagnetic down to low temperatures, thus avoiding large magnetoresistance effects. Gage resistance is 350 $\Omega$ at 300 K, and 321 $\Omega$ at 4.2 K.

The gage resistance is measured with an ac Wheatstone bridge operating at 400 Hz. Bridge unbalance signals are

[a] Supported by a fellowship from the Brazilian Conselho Nacional de Pesquisa Cientifica e Tecnologica.

 0021-8979/84/041073-08$02.40  

amplified with a Princeton Applied Research lock-in amplifier, Model HR-8, and displayed on a chart recorder. The active gage is attached to the actual ferromagnetic sample, and an identical dummy gage is attached to a dummy sample consisting of a copper disc, located in close proximity to the actual sample. The active gage and the dummy gage are in adjacent arms of the bridge, in order to cancel most of the effect of temperature and of magnetic field on the gages themselves.

The calibration factors of gages identical to those used in actual magnetostriction measurements are determined at 300, 77, and 4.2K, with an apparatus[9] generating known bending strains. The results agree within $\pm 2\%$ with the values given by the manufacturer, or with a linear extrapolation of the latter values down to 4.2 K. The strain gauges are made of several narrow conducting strips, here oriented parallel to the sample length. Using our calibration apparatus, we have explored the possibility that our gages might be sensitive to strains perpendicular to the length of the conducting strips. The answer is negative: only strains parallel to the conducting strips affect the gage resistance, within experimental error.

During magnetostriction measurements, the ends of the actual sample are glued to flexible brass strips normal to the sample length, which support the sample while allowing longitudinal magnetostrictive strains.

A magnetic field is applied in the plane of the sample. It can be rotated between two directions, one parallel and the other normal to the sample length.

At 4.2 and 77 K, the sample is immersed in baths of liquid helium and liquid nitrogen, respectively. At 300 K, the sample is in atmospheric air. Magnetothermal changes of sample temperature are observed at 300 K every time the magnetic field is changed, because of the absence of a bath. These transient changes are troublesome because they affect the gage resistance. To eliminate them, we wait 1–5 min after every field change, before recording the bridge output signal.

## III. EXPERIMENTAL RESULTS

As explained above, the strain gage measures magnetostrictive strains in a direction parallel to the sample length. When induced by a magnetization parallel to the sample length, this strain is denoted by $(\delta l/l)_{\parallel}$. For a magnetization normal to the sample length, the strain is $(\delta l/l)_{\perp}$. By defintion,[10] the linear magnetostriction at saturation is

$$\lambda_s = \tfrac{2}{3}\left[(\delta l/l)_{\parallel} - (\delta l/l)_{\perp}\right], \tag{1}$$

where $(\delta l/l)_{\parallel}$ and $(\delta l/l)_{\perp}$ are measured at fields sufficient to saturate the sample. This definition is appropriate for amorphous or polycrystalline samples. Our external field has a maximum value of 0.38 T. Usually, saturation is already achieved at 0.1 T.

The experimental values of $\lambda_s$ at 300 K are plotted as a function of iron concentration $x$ in Fig. 1. Note that $\lambda_s = 0$ for $x < 0.12$, because the Curie temperature is below 300 K. Similarly, the $\lambda_s$ data at 77 and 4.2 K are plotted on Figs. 2 and 3. The data for the annealed $x = 0.4$ and 0.5 samples are not shown, as we were unable to saturate these magnetically hard, tetragonal alloys.

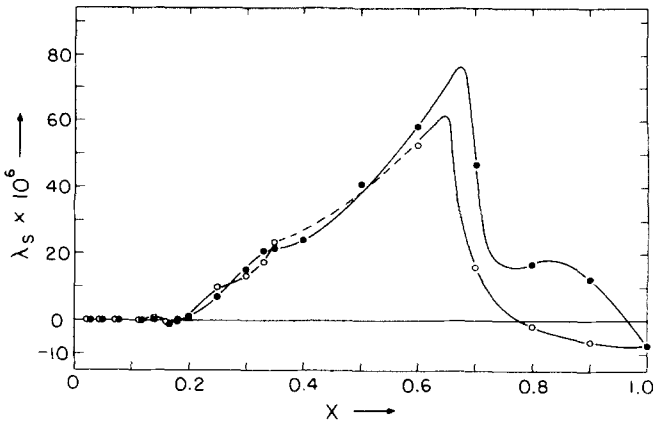


FIG. 1. Saturation magnetostriction at 300 K. Solid circles are for quenched alloys, and open circles for annealed alloys.

On Fig. 4, we compare our data with data from the literature,[1,3,4] in the case of quenched alloys at 300 K. In general, there is good agreement.

In the case of annealed alloys at 300 K (Fig. 5), the agreement with the data of the literature[3,4] is not very good. The field of $\simeq$0.06 T used in Refs. 3 and 4 may be too small to saturate certain annealed samples in the range of composition where the tetragonal face-centered phase exists. Also, the slow furnace cooling used by them does not produce complete atomic ordering. This is shown by the different $\lambda_s$ value obtained after a longer anneal[3] at 600 °C.

Only two data points at 4K are available from the literature[2] (Fig. 6). The agreement with our data is very good. This figure shows our data at 4.2 K in the $0 \leqslant x \leqslant 0.25$ range, on an expanded scale. We see that $\lambda_s$ goes through zero four times in that composition range. There are enough data points to show that this behavior is real, and not the result of experimental random errors.

## IV. SPLIT-BAND MODEL FOR TRANSITION METALS

Our data analysis is based on a simplified model[11,12] of the band structure, where each constituent of the alloy has its own $d$ band, distinct on the energy scale (Fig. 7). This

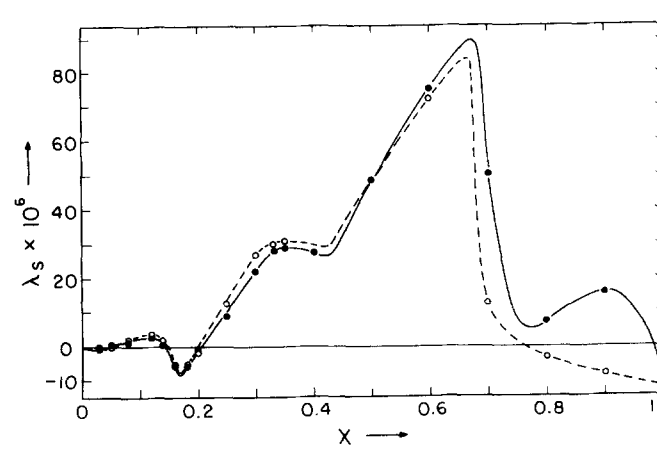


FIG. 2. Saturation magnetostriction at 77 K. Solid circles are for quenched alloys, and open circles for annealed alloys.

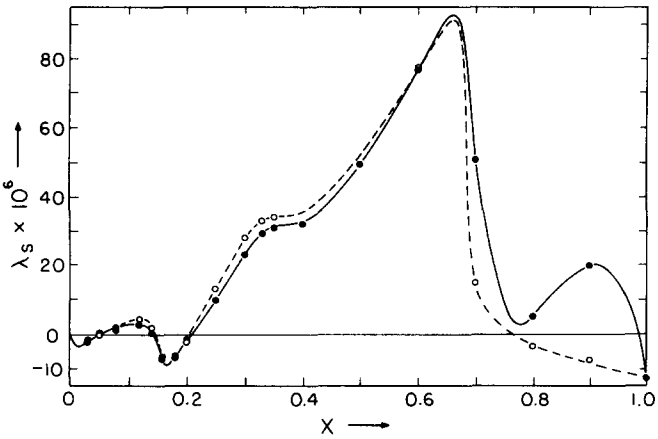


FIG. 3. Saturation magnetostriction at 4.2 K. Solid circles are for quenched alloys, and open circles for annealed alloys.

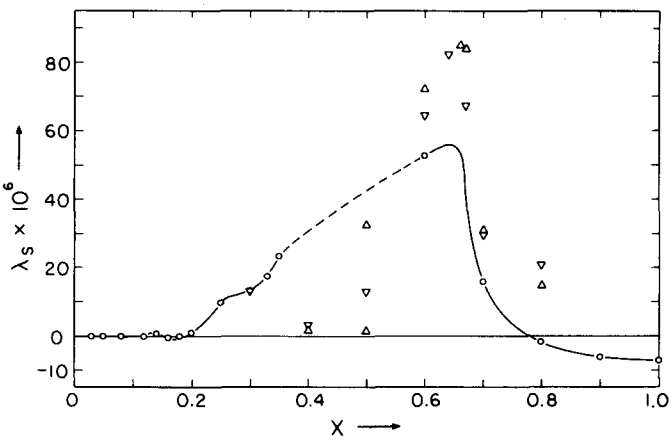


FIG. 5. Saturation magnetostriction at 300 K for annealed alloys, compared to data from the literature. Open circles: our data. △ symbols: data from Ref. 3. ∇ symbols: data from Ref. 4.

split-band model is valid when the difference of valence of the constituent atoms is sufficiently large. This model has already been applied[11] to the magnetostriction, anomalous Hall effect, $g$ factor, and electronic specific heat of Ni-Fe alloys, and also to the magnetostriction,[13] anomalous Hall effect,[14] and electronic specific heat[15] of amorphous Ni-Fe-base ribbons.

In the split-band model for Pd-Fe alloys (Fig. 7), the number of states in the spin-down iron band is $5x$, and the number of states in the spin-down palladium band is $5(1-x)$, as for ordinary atomic $d$ states. Similar expressions hold for the spin-up bands.

The simplest case, realized at $0.20 < x < 0.68$, is the one where the spin-up $d$ bands are full [Fig. 7(a)] and contain a total of five electrons per atom. Then, the number of electrons in the spin-down band is

$$n_e^{\downarrow} = n_e - 5, \tag{2}$$

where $n_e$ is the number of $d$ electrons in the alloy, related to the number $n_e^{\mathrm{Pd}}$ for pure palladium by

$$n_e = n_e^{\mathrm{Pd}} - 2x. \tag{3}$$

Here, $-2$ is the difference of valence between iron and palladium. By combining the two last equations, we obtain

$$n_e^{\downarrow} = n_e^{\mathrm{Pd}} - 5 - 2x. \tag{4}$$

The saturation magnetization, expressed in Bohr magnetons per atom, is

$$n_B = \frac{g}{2}(5 - n_e^{\downarrow}) = \frac{g}{2}(10 - n_e^{\mathrm{Pd}} + 2x), \tag{5}$$

where $g$ is the $g$-factor obtained from ferromagnetic resonance data.[16] Equation (5) predicts $n_B$ to be a linear function of $x$ with a slope of $+2$, in agreement with existing magnetization data[17] for Pd-Fe at $0.20 < x < 0.68$. In turn, this Slater–Pauling behavior confirms that the spin-up bands are full in that composition range, as assumed here. Also, by fitting Eq. (5) to the magnetization data, we obtain $n_e^{\mathrm{Pd}} = 9.49$ electron/atom = const.

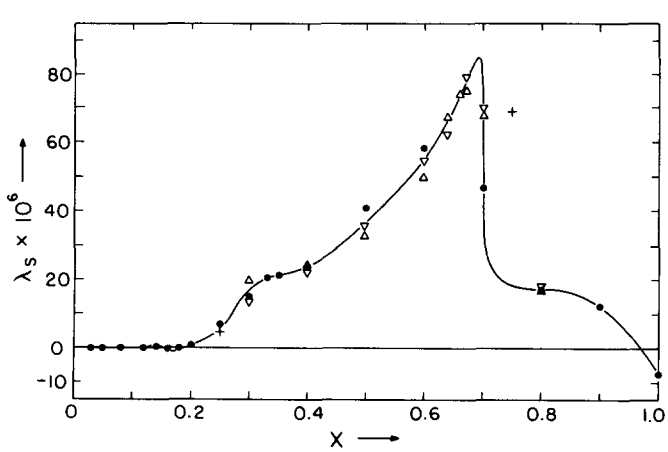


FIG. 4. Saturation magnetostriction at 300 K for quenched alloys, compared to data from the literature. Solid circles: our data. Crosses: data from Ref. 1. △ symbols: data from Ref. 3. ∇ symbols: data from Ref. 4.

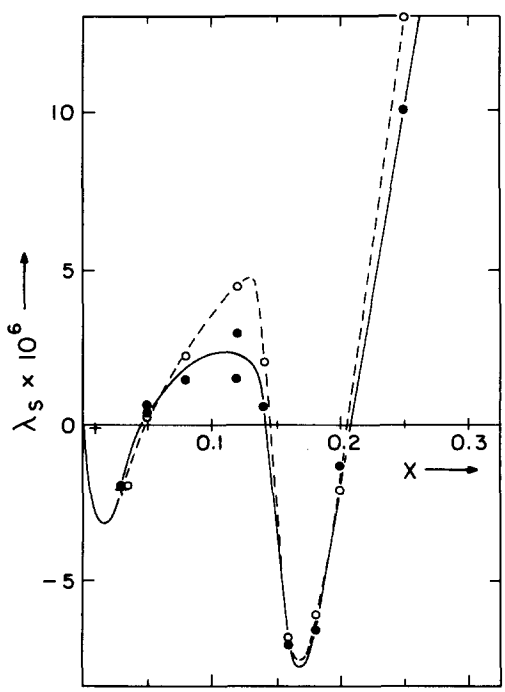


FIG. 6. Saturation magnetostriction at 4.2 K for $0 < x < 0.25$. Solid circles: our data for quenched alloys. Open circles: our data for annealed alloys. Crosses: data from Ref. 2.

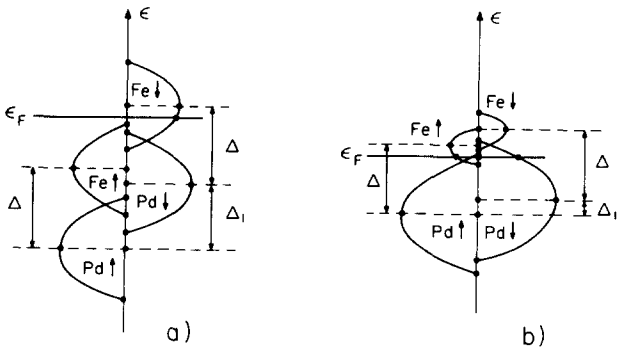


FIG. 7. (a) Split-band model for $Pd_{1-x}Fe_x$ at $x > 0.2$, where the spin-up bands are full. (b) At $x < 0.2$, the spin-up bands are not full.

In the range of low iron concentration $x < 0.20$, the spin-up $d$ band is not full, and contains an unknown number $n_e^{\uparrow}$ of electrons [Fig. 7(b)]. Equation (2) is replaced by

$$n_e^{\uparrow} + n_e^{\downarrow} = n_e. \tag{6}$$

Also, Eq. (5) is replaced by

$$n_B = \frac{g}{2}(n_e^{\uparrow} - n_e^{\downarrow}). \tag{7}$$

Using Eqs. (3), (6), and (7), we obtain

$$n_e^{\uparrow} = \tfrac{1}{2}(n_B + n_e^{Pd} - 2x),$$
$$n_e^{\downarrow} = \tfrac{1}{2}(n_e^{\mathrm{Pd}} - 2x - n_B). \tag{8}$$

De Haas–Van Alphen data[18] for pure Pd suggest 0.36 $s$ electrons per atom. This implies $n_e^{\mathrm{Pd}} = 10 - 0.36 = 9.64$ electron/atom, in disagreement with the value of 9.49 used above for $x > 0.20$. Presumably, $n_e^{\mathrm{Pd}}$ varies in the $0 < x < 0.20$ range, because of a shift of the $s$ band with respect to the $d$ band. We will use a simple linear expression in that range, for interpolation:

$$n_e^{\mathrm{Pd}} = 9.64 - 0.79x \quad (0 < x < 0.20). \tag{9}$$

## V. BAND THEORY OF MAGNETOSTRICTION

In the case of itinerant $d$ states, spin-orbit interaction can be written[19] in the approximate form

$$H_{so} \simeq \sum_{\mathbf{l}} \xi_l(|\mathbf{r} - \mathbf{l}|)\,[\mathbf{p} \times (\mathbf{r} - \mathbf{l})]\cdot\mathbf{S}, \tag{10}$$

where $\mathbf{l}$ denotes the crystal sites, $\mathbf{p}$ the momentum, and $\mathbf{S}$ the spin,

$$\xi_l(r) = \frac{\hbar^2}{2m^2c^2}\frac{1}{r}\frac{dV_l(r)}{dr}, \tag{11}$$

and $V_l(r)$ is the electric potential energy, assumed to be approximately central close to each atomic site l. In an alloy, $V_l(r)$ and $\xi_l(r)$ may differ at sites l having chemically different atoms.

The energy $\epsilon$ of each band state of symmetry $n$ ($n = 1$–5 for $d$ states), spin $\chi$ (↑ or ↓), and belonging to the $i$th band of the split-band model (Fe or Pd band), suffers a shift $\delta\epsilon_{\mathrm{so}}^{ni\chi}$ when spin-orbit interaction is switched on. The total energy shift for the electron sea is

$$\delta E_{\mathrm{so}} = \sum_n \sum_i \sum_\chi \int_{-\infty}^{\epsilon_{Fo}} N_0^{ni\chi}(\epsilon)\,\delta\epsilon_{\mathrm{so}}^{ni\chi}(\epsilon,\hat{\alpha})\,d\epsilon, \tag{12}$$

where $\epsilon_{Fo}$ is the unperturbed Fermi level, $N_0^{ni\chi}$ the unperturbed density of states, and $\hat{\alpha}$ the unit vector parallel to the magnetization.

A bunching of states on the energy scale occurs if $\delta\epsilon_{\mathrm{so}}^{ni\chi}$ depends on the energy. The new density of states[20] is

$$N_{\mathrm{so}}^{ni\chi} = N_0^{ni\chi} - \frac{d}{d\epsilon}(N_0^{ni\chi}\,\delta\epsilon_{\mathrm{so}}^{ni\chi}). \tag{13}$$

Then we switch on a constant-volume (pure shear) elastic strain of the lattice. We assume it to be uniaxial, and thus described by one number $\lambda_s$. The strain $\lambda_s$ alters the energy of one state by $\delta\epsilon_d^{ni}$. The total shift for the electron sea is

$$\delta E_d = \sum_n \sum_i \sum_\chi \int_{-\infty}^{\epsilon_F^{\mathrm{so}}} N_{\mathrm{so}}^{ni\chi}(\epsilon)\,\delta\epsilon_d^{ni}(\epsilon)\,d\epsilon, \tag{14}$$

where $\epsilon_F^{\mathrm{so}}$ is the Fermi level in the presence of spin-orbit interaction.

We assume $\delta\epsilon_d^{ni}$ to be proportional to $\lambda_s$, and the coefficient of proportionality defines the deformation potential $V^{ni}(\hat{\beta})$.

$$\delta\epsilon_d^{ni} = \lambda_s V^{ni}(\hat{\beta}). \tag{15}$$

Here, $\hat{\beta}$ is the unit vector in the direction of the uniaxial strain. Using Eqs. (12)–(15), we calculate the total shift $\delta E_{\mathrm{so}} + \delta E_d$. Assuming that $V^{ni}(\hat{\beta})$ does not depend on $\epsilon$ or on the band index $i$, one can show that the result is independent of the order in which $\delta E_{\mathrm{so}}$ and $\delta E_d$ are switched on.

We keep only the term which depends simultaneously on the strain and on the magnetization direction, called magnetoelastic energy $E_{\mathrm{me}}$. Assuming $N_o^{ni\chi}(-\infty) = 0$, and integrating over energy, we obtain[20]

$$E_{me} = -\lambda_s \sum_n \sum_i \sum_\chi V^{ni}(\hat{\beta})\,N_0^{ni\chi}(\epsilon_F^{\mathrm{so}})\,\delta\epsilon_{so}^{ni\chi}(\epsilon_F^{\mathrm{so}},\hat{\alpha}). \tag{16}$$

We see that the magnetoelastic energy depends on the density of states and spin-orbit shift at the Fermi level.[20]

To this, we add the ordinary elastic energy, proportional to $\lambda_s^2$, where $Y_s$ is the shear modulus, and $v$ the crystal volume:

$$E_{\mathrm{el}} = \frac{Y_s}{2}\lambda_s^2 v. \tag{17}$$

For simplicity, and in order to minimize the number of adjustable parameters, we take into account only $d$ states with $t_{2g}$ symmetry ($n = 1, 2, 3$). This is permissible if these states are dominant at the Fermi level, or if we are only interested in a rough theory to explain the composition dependence of $\lambda_s$. The probability density for such states has a fourfold symmetry axis parallel to one of the cubic crystal axes ($x, y, z$). As a result, the deformation potentials can be shown to have the form

$$V^{1i}(\hat{\beta}) = -p(3\hat{\beta}_x^2 - 1),$$
$$V^{2i}(\hat{\beta}) = -p(3\hat{\beta}_y^2 - 1), \tag{18}$$
$$V^{3i}(\hat{\beta}) = -p(3\hat{\beta}_z^2 - 1),$$

where $p$ is a constant.

The density of states assumed for the iron band and palladium band has the simple form[11] (Fig. 7):

$$N_0^{n\,\mathrm{Fe}\uparrow}(\epsilon)=\frac{2.5}{w_{\mathrm{Fe}}}x^{1/2}\left[1-\left(\frac{2(\epsilon-\Delta-\Delta_1)}{x^{1/2}w_{\mathrm{Fe}}}\right)^2\right]$$
$$(|\epsilon-\Delta-\Delta_1|<\tfrac{1}{2}x^{1/2}w_{\mathrm{Fe}});$$
$$N_0^{n\,\mathrm{Pd}\uparrow}(\epsilon)=\frac{2.5}{w_{\mathrm{Pd}}}(1-x)^{1/2}\left[1-\left(\frac{2(\epsilon-\Delta_1)}{(1-x)^{1/2}w_{\mathrm{Pd}}}\right)^2\right]$$
$$(|\epsilon-\Delta_1|<\tfrac{1}{2}(1-x)^{1/2}w_{\mathrm{Pd}});\qquad(19)$$
$$N_0^{n\,\mathrm{Fe}\downarrow}(\epsilon)=\frac{2.5}{w_{\mathrm{fe}}}x^{1/2}\left[1-\left(\frac{2(\epsilon-\Delta)}{x^{1/2}w_{\mathrm{Fe}}}\right)^2\right]$$
$$(|\epsilon-\Delta|<\tfrac{1}{2}x^{1/2}w_{\mathrm{Fe}});$$

$$N_0^{n\,\mathrm{Pd}\downarrow}(\epsilon)=\frac{2.5}{w_{\mathrm{Pd}}}(1-x)^{1/2}\left[1-\left(\frac{2\epsilon}{(1-x)^{1/2}w_{\mathrm{Pd}}}\right)^2\right]$$
$$(|\epsilon|<\tfrac{1}{2}(1-x)^{1/2}w_{\mathrm{Pd}}).$$

Outside the intervals of $\epsilon$ indicated, all these densities of states are equal to zero. Also, $\Delta$ is the separation between the centers of the Pd and Fe bands, $\Delta_1$ is the exchange splitting, and $w_{\mathrm{Fe}}$ and $w_{\mathrm{Pd}}$ are the pure-metal band widths. These densities of states have been renormalized to compensate for the exclusion of the $e_g$ states, so that the total number of $d$ states adds up to 5 electrons/spin atom.

## VI. TIGHT-BINDING FORMALISM

The alloy $d$ states $\psi_{\epsilon\chi}^{in}$ of energy $\epsilon$ are written as linear combinations of atomic orbitals $\phi_n^{\,l}$. The $\phi_n^{\,l}$ are assumed real valued:

$$\psi_{\epsilon\chi}^{in}(\mathbf{r})=\sum_{\mathbf{l}}C_{\epsilon\chi}^{in}(\mathbf{l})\phi_n^{\,l}(\mathbf{r}-\mathbf{l})\,K(\chi),\qquad(20)$$
$$\phi_n^{\,l}(\mathbf{r})=R^l(r)\theta_n(\theta,\phi).$$

We use second-order perturbation theory to calculate $\delta\epsilon_{\mathrm{so}}^{ni\chi}$. The spin quantization axis is assumed to be along the $z$ cubic crystal axis. We obtain, for a spin-up state as an example

$$\delta\epsilon_{\mathrm{so}}^{ni\uparrow}=\sum_j\sum_k\tfrac{1}{4}\Big|\sum_{\mathbf{l}}C_{\epsilon\uparrow}^{in*}(\mathbf{l})C_{\epsilon\uparrow}^{jk}(\mathbf{l})\xi^l\Big|^2$$
$$\times(L_z^{\,nk}G_k^{j\uparrow}+L_+^{\,nk}G_k^{j\downarrow})$$
$$G_k^{j\chi}(\epsilon)=\int_{-\infty}^{+\infty}\frac{N_0^{jk\chi}(\epsilon')}{\epsilon-\epsilon'}\,d\epsilon',\qquad(21)$$
$$L_z^{\,nk}=|\langle\theta_n|L_z|\theta_k\rangle|^2;\quad L_{\pm}^{\,nk}=|\langle\theta_n|L\pm|\theta_k\rangle|^2;$$
$$\xi^l=\langle R^l|\xi_l(r)|R^l\rangle.$$

In this $\delta\epsilon_{\mathrm{so}}^{ni\uparrow}$ expression, we have kept only the terms where $\theta_n$, $\theta_k$, and $\xi^l$ refer to the same crystal site, since $\xi_l(r)$ is a local operator. Also, we have assumed the squares $|C_{\epsilon\uparrow}^{in}(\mathbf{l})|^2$ and the radial functions $R^l(r)$ to be independent of $\chi$ and $\epsilon$. Recall that $i,j$ are band indexes, and $n,k$ denote state symmetry. We drop the $\epsilon$ and $\chi$ subscripts in the $C$ coefficients.

When expanding the square of the sum in the $\delta\epsilon_{\mathrm{so}}^{ni\uparrow}$ of Eq. (21), products such as $C^{in*}(\mathbf{l}_1)C^{jk}(\mathbf{l}_1)C^{in}(\mathbf{l}_2)C^{jk*}(\mathbf{l}_2)$, where $\mathbf{l}_1$ and $\mathbf{l}_2$ are two different values of $\mathbf{l}$, can be neglected since the complex phases of the $C$ coefficients are spatially random in disordered alloys. Only the square terms remain.

By combining Eqs. (16)–(18), and (21), and evaluating $L_z^{\,nk}$ and $L_{\pm}^{\,nk}$, we obtain

$$E_{me}+E_{el}=\frac{Y_s}{2}v\lambda_s^{\,2}-\sum_i\sum_{\chi}\lambda_s[1-3(\hat{\beta}\cdot\hat{\alpha})^2]$$
$$\times p(\delta\epsilon_{\mathrm{so}}^{3i\chi}-\delta\epsilon_{\mathrm{so}}^{1i\chi})N_o^{1i\chi}(\epsilon_F^{\mathrm{so}}).\qquad(22)$$

We minimize $E_{me}+E_{el}$ with respect to $\hat{\beta}$ and $\lambda_s$. This gives the equilibrium strain:

$$\hat{\beta}=\pm\hat{\alpha},$$
$$\lambda_s=\frac{1}{Y_s v}\sum_i\sum_{\chi}2p\,N_o^{1i\chi}(\epsilon_F^{\mathrm{so}})(\delta\epsilon_{\mathrm{so}}^{1i\chi}-\delta\epsilon_{\mathrm{so}}^{3i\chi}).\qquad(23)$$

As a further rough approximation, we consider the terms referring to various iron sites to be equal, and similarly at palladium sites. The symbols Ir and Pa label these sites, by opposition to the band symbols Fe and Pd. For example, $|C^{\mathrm{Fe}\,n}(\mathrm{Pa})|^2$ is the probability of finding a Fe-band electron at a palladium site. The energy shift becomes, for example:

$$\delta\epsilon_{\mathrm{so}}^{n\mathrm{Fe}\uparrow}\simeq\sum_k\frac{n_{\mathrm{at}}}{4}[X\xi^2(\mathrm{Ir})|C^{\mathrm{Fe}n}(\mathrm{Ir})|^2|C^{\mathrm{Fe}k}(\mathrm{Ir})|^2+(1-X)\xi^2(\mathrm{Pa})|C^{\mathrm{Fe}n}(\mathrm{Pa})|^2|C^{\mathrm{Fe}k}(\mathrm{Pa})|^2)$$
$$\times(L_z^{\,nk}G_k^{\mathrm{Fe}\uparrow}+L_+^{\,nk}G_k^{\mathrm{Fe}\downarrow})+[x|C^{\mathrm{Fe}\,n}(\mathrm{Ir})|^2|C^{\mathrm{Pd}\,k}(\mathrm{Ir})|^2\xi^2(\mathrm{Ir})+(1-x)|C^{\mathrm{Fe}\,n}(\mathrm{Pa})|^2|C^{\mathrm{Pd}k}(\mathrm{Pa})|^2\xi^2(\mathrm{Pa})]$$
$$\times(L_z^{\,nk}G_k^{\mathrm{Pd}\uparrow}+L_+^{\,nk}G_k^{\mathrm{Pd}\downarrow})],\qquad(24)$$

where $n_{\mathrm{at}}$ is the total number of atoms in the crystal.

The normalization condition gives

$$n_{\mathrm{at}}x|C^{\mathrm{Fe}\,n}(\mathrm{Ir})|^2+n_{\mathrm{at}}(1-x)|C^{\mathrm{Fe}\,n}(\mathrm{Pa})|^2=1,$$
$$n_{\mathrm{at}}x|C^{\mathrm{Pd}\,n}(\mathrm{Ir})|^2+n_{\mathrm{at}}(1-x)|C^{\mathrm{Pd}\,n}(\mathrm{Pa})|^2=1.\qquad(25)$$

The completeness condition for the $d$ band gives

$$n_{\mathrm{at}}x|C^{\mathrm{Fe}\,n}(Ir)|^2+n_{\mathrm{at}}(1-x)|C^{\mathrm{Pd}\,n}(\mathrm{Ir})|^2=1;$$
$$n_{\mathrm{at}}x|C^{\mathrm{Fe}\,n}(Pa)|^2+n_{\mathrm{at}}(1-x)|C^{\mathrm{Pd}\,n}(\mathrm{Pa})|^2=1.\qquad(26)$$

The determinant of the four Eqs. (25) and (26) vanishes, so that the $C$ coefficients cannot be determined completely. These equations give, however

$$\frac{|C^{\mathrm{Pd}n}(\mathrm{Ir})|^2}{(1-x)[\,|C^{\mathrm{Pd}n}(\mathrm{Pa})|^2-|C^{\mathrm{Pd}n}(\mathrm{Ir})|^2]} = \frac{|C^{\mathrm{Fe}n}(\mathrm{Pa})|^2}{x[\,|C^{\mathrm{Fe}n}(\mathrm{Ir})|^2-|C^{\mathrm{Fe}n}(\mathrm{Pa})|^2]} = K_0. \tag{27}$$

Arbitrarily, we will assume the common value $K_0$ of these two fractions to be independent of composition. This assumption has at least the merit of being symmetric with respect to the two components of the alloy.

For the $d$ band widths,[21,22] we use $w_{\mathrm{Pd}} = 5.45$ eV, $w_{\mathrm{Fe}} = 4.87$ eV. These are the distances between extreme top and bottom of the band of the pure metal.

For the spin-orbit parameters, we use the atomic values[23] $\xi(\mathrm{Ir}) = 0.04848$ eV and $\xi(\mathrm{Pa}) = 0.175$ eV. The shear modulus $Y_s$ is related by $Y_s = 3Y/2(1+\nu)$ to the Young modulus $Y$ measured in Ref. 4, and to the Poisson ratio $\nu \simeq 1/3$. The crystal volume $v$ is derived from the lattice parameter.[24]

Numerical calculations of $\lambda_s$ are done with a computer in the following manner. For each value of $x$, $n_e^{\uparrow}$ and $n_e^{\downarrow}$ are obtained from existing $n_B$ data[17] by Eqs. (8), or by Eqs. (4) and (9). Then, the Fermi levels for spin-up and spin-down electrons are found in the bands of Eqs. (19). In turn, this fixes $\Delta_1$. Using Eqs. (25) and (27), the squared $C^{in}$ coefficients are evaluated, and substituted into Eq. (24). The $G_k^{ix}$ functions are calculated analytically from Eq. (21) and (19), and also substituted into Eq. (24). Finally, the spin-orbit shifts of Eq. (24) are substituted into the $\lambda_s$ expression of Eq. (23).

This procedure is repeated to find the values of $\Delta$, $K_0$, and $p$ giving the best fit to our $\lambda_s$ data at 4 $K$. These are $\Delta = 2.6$ eV, $p = -0.6$ eV, $K_0 = 1.5$ (Fig. 8). Overall, the theoretical $\lambda_s$ curve is in fair agreement with the experimental curve. In particular, the theoretical curve shows the same number of changes of sign as the experimental curve. Note that our theory is meant to apply only to the fcc region ($x < 0.7$ for quenched alloys).

According to our theory, the several observed changes of sign of $\lambda_s$ are caused by the successive passages through the Fermi level of the spin-up iron band and spin-up palladium band (Fig. 7), as the alloy becomes magnetized at increasing $x$, in the range $x < 0.3$. Also, the observed positive sign of $\lambda_s$ at $x > 0.21$ is caused[11] by the Fermi level being in the lower half of the spin-down iron band [Fig. 7(a)], and the spin-up bands being full. Note that the sign of $\lambda_s$ is mediated[11] by the sign of the Green's functions of Eqs. (21).

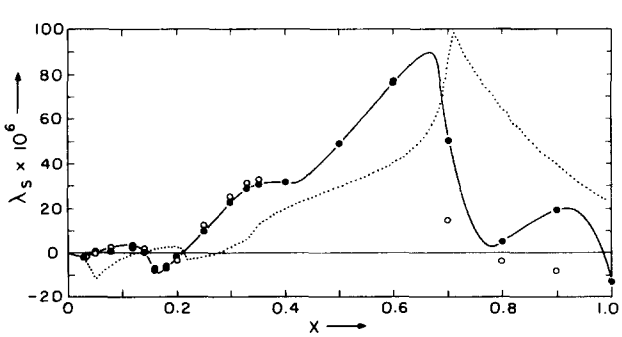


FIG. 8. Dotted line: theoretical values of magnetostriction at 0 K. Solid circles: our data for quenched alloys at 4.2 K. Open circles: our data for annealed alloys at 4.2 K.

## VII. CALCULATION OF OTHER PHYSICAL QUANTITIES

Now, we treat the anomalous Hall conductivity $\gamma_{Hs}$. As shown earlier,[11] it appears that $\gamma_{Hs}$ is proportional to $\langle L_z \rangle(\epsilon_F)$, the expectation of $L_z$ for states at the Fermi level. Using the Green's functions of Eqs. (21), this implies the approximate expression, without spin-flip terms:

$$\gamma_{Hs} \simeq B\,[N_0^{\mathrm{Fe}\uparrow}(\epsilon_{\mathrm{F0}})G_k^{\mathrm{Fe}\uparrow}(\epsilon_{\mathrm{F0}}) - N_0^{\mathrm{Fe}\downarrow}(\epsilon_{\mathrm{Fo}})G_k^{\mathrm{Fe}\downarrow}(\epsilon_{\mathrm{F0}}) + N_0^{\mathrm{Pd}\uparrow}(\epsilon_{\mathrm{F0}})G_k^{\mathrm{Pd}\uparrow}(\epsilon_{\mathrm{F0}}) - N_0^{\mathrm{Pd}\downarrow}(\epsilon_{\mathrm{F0}})G_k^{\mathrm{Pd}\downarrow}(\epsilon_{\mathrm{F0}})], \tag{28}$$

where $B$ is a constant coefficient. Using the same parameter values as before, and $B = 10^6\ \Omega^{-1}\ \mathrm{m}^{-1}$, Eq. (28) gives the theoretical curve of Fig. 9. On the same figure, we give the experimental values $\gamma_{Hs} = R_s M_s/\rho^2$, where the anomalous Hall coefficient $R_s$ is from Ref. 25, and the resistivity $\rho$ from Ref. 26. There is fair agreement between theory and experiments. Note that our theory predicts correctly that there is only one change of sign of $\gamma_{Hs}$. The behaviors of $\lambda_s$ and $\gamma_{Hs}$ differ in that respect, because the Hall effect is odd in the spin direction, leading to minus signs for the spin-down Green's functions in Eq. (28). This difference between $\lambda_s$ and $\gamma_{Hs}$ becomes inoperative[11] in Ni-Fe, Ni-Co, Ni-Fe-Cu, etc., where the spin-up band is full, and only states of one spin matter. Then, both $\lambda_s$ and $\gamma_{Hs}$ have only one sign change, located at the composition where the spin-down Fermi level moves from the nickel band to the iron band.

Another quantity depending on spin-orbit interaction is the $g$-factor. The total orbital angular momentum $\Sigma L_z$ of the Fermi sea (per atom) can be derived[11] from it by the relation

$$\Sigma L_z = \left(1 - \frac{2}{g}\right) n_B. \tag{29}$$

From existing $g$ data[16] for Pd-Fe, we have calculated $\Sigma L_z$ by Eq. (29) (Fig. 10). We see that $\Sigma L_z$ has a minimum at the iron concentration $x \simeq 0.15$. As in Ni-Fe, the minimum is at the approximate composition[11] where the spin-down Fermi level moves from the palladium (or nickel) band to the iron band. The existence and location of such a minimum is correctly predicted[11] by our split-band model.

From the density of states of Eqs. (19), we have also calculated the electronic specific heat coefficient $\gamma$. It is in good agreement with existing $\gamma$ data for Pd-Fe, provided a

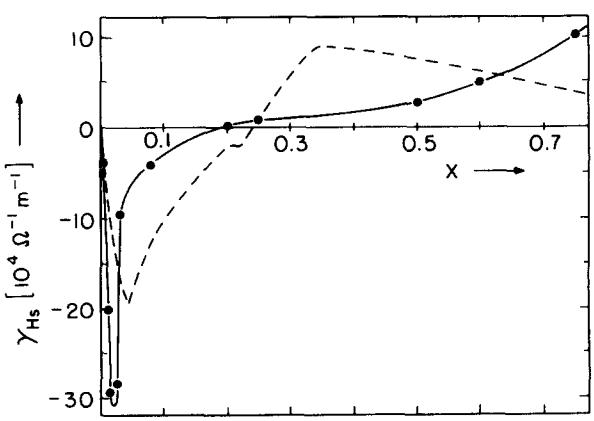


FIG. 9. Dashed line: theoretical values of anomalous Hall conductivity. Solid circles: data from Ref. 25, at 0 K, for quenched alloys.

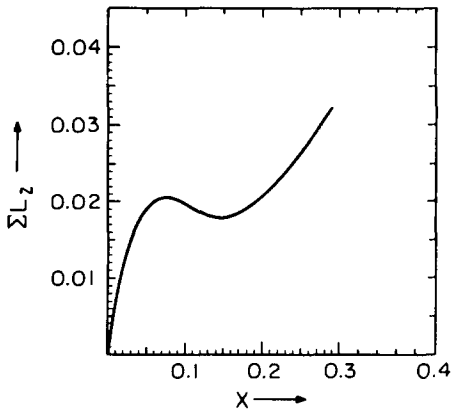


FIG. 10. Experimental values of the total orbital angular momentum of the Fermi sea at 0 K, plotted vs iron concentration. These values are derived from the $g$-factor data of Ref. 16, and exhibit a minimum at $x = 0.15$.

value $\lambda \simeq 0.5$ of the electron-phonon or electron-magnon enhancement factor is assumed. This is a reasonable value for transition metals. Finally, from the $C$ coefficients, of Eqs. (25)–(27), we have calculated the local iron moments and palladium moments. They are in semiquantitative agreement with existing neutron diffraction data. For example, the iron moment is correctly predicted to be much larger than the palladium moment. All this confirms the general reasonableness of our theory.

## VIII. CONCLUSIONS AND FINAL REMARKS

We have measured the linear magnetostriction $\lambda_s$ of Pd-Fe alloys at 300, 77, and 4.2 K. The effect of atomic ordering on $\lambda_s$ has been investigated. Although $\lambda_s$ is positive for most iron atomic fractions $x > 0.21$, it oscillates and undergoes repeated changes of sign at $x < 0.21$. These unusual oscillations are probably related to the successive passages of the spin-up palladium $d$ band and spin-up iron $d$ band through the Fermi level, as the iron concentration increases and the $d$ band becomes magnetized.

A simple "split-band" model, where the palladium and iron $d$ bands are distinct on the energy scale, is able to reproduce most features of our $\lambda_s$ data, including the oscillations. It is used in conjunction with a deformation-potential theory of magnetostriction in metals.

Presumably, better agreement between theory and $\lambda_s$ data could be achieved if a more complicated shape of the density of states of the palladium and iron bands were assumed. The predicted locations of the zeros of $\lambda_s$ might be more accurate. An asymmetric $d$ band shape has been used by Onn,[15] to represent electronic specific heat data within the split-band model.

Another defect of our simple theory is the assumption that all $d$ states have the same symmetry as $t_{2g}$ atomic states. Also, we have assumed the deformation potential to be independent of band energy. Finally, the spin magnetization has been assumed to be along one of the cubic axes, which is not realistic in a polycrystal. Our theory is only designed to explain the compositional dependence of $\lambda_s$.

On the other hand, the present theory is more general than the ones of Refs. 11 and 12, because it takes into account both spin-up and spin-down states.

## ACKNOWLEDGMENTS

We thank Dr. Y. Hsu and S. Jen for making some of the samples used here. Also, we used the facilities of the CMU Center for the Joining of Materials. Dr. R. C. O'Handley gave us useful information on strain gages at the beginning of the work. An atomic absorption spectrophotometer used for sample analysis was paid by NSF grant DMR-800 1662, and made available by the Carnegie-Mellon Department of Metallurgy and Materials Science.

[1]Z. I. Alizade, Vestnik Moskovskogo Universiteta **9**, 67 (1950); Dokl. Akad. Nauk SSSR **73**, 79 (1950).
[2]E. Fawcett, D. B. McWhan, and R. C. Sherwood, Solid State Commun. **6**, 509 (1968).
[3]K. Fukamichi, J. Appl. Phys. **50**, 6562 (1979).
[4]T. Nakayama, M. Kikuchi, and K. Fukamichi, J. Phys. F (London) **10**, 715 (1980); IEEE Trans. Magn. **MAG-16**, 1071 (1980).
[5]M. H. Lee, J. M. Eldridge, and W. Y. Lee, J. Appl. Phys. **49**, 1986 (1978).
[6]Y. Hsu, J. E. Schmidt, M. Gupta, S. Jen, and L. Berger, J. Appl. Phys. **54**, 1887 (1983).
[7]E. Raub, H. Beeskow and O. Loebich, Z. Metallkd. **54**, 549 (1963); A. Kussmann and K. Jessen, Z. Metallkd. **54**, 504 (1963); A. Z. Menshikov, G. P. Gasnikova, Yu. A. Dorofeyev, S. K. Sidorov, and V. A. Tsurin, Phys. Met. Metallogr. **44**, 17 (1978).
[8]J. E. Goldman, Trans. ASM **37**, 212 (1946); H. Zijlstra, *Experimental Methods in Magnetism*, Part 2 (Interscience, New York, 1967) p. 146; R. C. Dove and P. H. Adams, *Experimental Stress Analysis and Motion Measurements* (Charles E. Merril, Ohio, 1964).
[9]R. M. McClintock, Rev. Sci. Instrum. **30**, 715 (1959).
[10]E. W. Lee, Rep. Pro. Phys. **18**, 184 (1955); R. R. Birss, Adv. Phys. **8**, 252 (1959).
[11]L. Berger, Physica **91B**, 31 (1977).
[12]H. Ashworth, D. Sengupta, G. Schnakenberg, L. Shapiro, and L. Berger, Phys. Rev. **185**, 792 (1969).
[13]R. C. O'Handley and L. Berger, Inst. Phys. Conf. Proc. (London) **39**, 477 (1978); R. C. O'Handley, Phys. Rev. B **18**, 930 (1978).
[14]R. C. O'Handley, Phys. Rev. B **18**, 2577 (1978).
[15]D. G. Onn, J. Appl. Phys. **52**, 1788 (1981).
[16]D. L. Hardison and E. D. Thompson, J. Phys. (Paris) **32**, C1-565 (1971); D. M. S. Bagguley and J. A. Robertson, Phys. Lett. **27A**, 516 (1968); J. Phys. F (London) **4**, 2282 (1974).
[17]J. W. Cable, E. O. Wollan, and W. C. Koehler, Phys. Rev. **138A**, 755 (1965); H. Fujimori and H. Saito, J. Phys. Soc. Jpn. **20**, 293 (1965); S. K. Sidorov, A. Z. Menshikov, and V. A. Kazantsev, Phys. Met. Metallogr. **34**, 72 (1972); J. Crangle, Philos. Mag. **5**, 335 (1960); B. H. Yeh, J. Chen, P. K. Tseng, and S. H. Fang, Chin. J. Phys. (Taiwan) **13**, 1 (1975); L. F. Abramova, G. V. Fedorov, and N. V. Volkensteyn, Phys. Met. Metallogr. **36**, 43 (1973); W. C. Phillips, Phys. Rev. **138A**, 1649 (1965); M. Fallot, Ann. Phys. (Paris) **10**, 291 (1938); M. Matsui, T. Shimizu, H. Yamada, and K. Adachi, J. Mag. Magn. Mater. **15–18**, 1201 (1980); D. Gerstenberg, Ann. Phys. **2**, 236 (1958).
[18]L. R. Windmiller, J. B. Ketterson, and S. Hornfeldt, Phys. Rev. B **3**, 4213 (1971).
[19]H. Brooks, Phys. Rev. **58**, 909 (1940); G. C. Fletcher, Proc. Phys. Soc. (London) Ser. A. **65**, 192 (1952), **67**, 505 (1954).
[20]L. Berger, Phys. Rev. **138**, A1083 (1965).
[21]A. D. McLachlan, J. G. Jenkin, R. C. G. Leckey, and J. Liesengang, J. Phys. F. (London) **5**, 2415 (1975); G. M. Stocks, R. W. Williams, and J. S. Faulkner, J. Phys. F (London) **3**, 1688 (1973); S. Hufner, G. K. Wertheim, and J. H. Wernick, Phys. Rev. B **8**, 4511 (1973); P. Oelhafen, E. Hauser, and H. J. Guntherrodt, Phys. Rev. Lett. **43**, 1135 (1979).
[22]S. Wakoh and J. Yamashita, J. Phys. Soc. Jpn. **21**, 1712 (1966); K. J. Duff and T. P. Das, *Electronic Density of States* (U.S. Dept. of Commerce, Publ. 323, 1969), p. 47; S. Asano and J. Yamashita, Tech. Rep. ISSP (Tokyo), Ser. A, No. 539 (1972); M. Singh, C. S. Wang, and J. Calloway, Phys. Rev. B **9**, 4897 (1972).
[23]J. Griffith, *The Theory of Transition Metal Ions* (Cambridge University, Cambridge, 1961), p. 106.

[24]R. Hocart and M. Fallot, C. R. Acad. Sci. (Paris) **204**, 1465 (1937); Z. Kristall. **99**, 509 (1938); E. Raub, H. Beeskow, and O. Loebich, Z. Metallkd. **54**, 549 (1963); R. Hultgren and C. A. Zapffe, AIME Trans. **133**, 58 (1939).

[25]L. I. Abramova, G. V. Fedorov, and N. V. Volkenshteyn, Phys. Metal. Metallogr. **38**, 79 (1974).

[26]L. I. Abramova, G. V. Fedorov, and N. V. Volkenshteyn, Phys. Metal. Metallogr. **33**, 527 (1972).